

# Brownian Dynamics Simulation for Modeling Ion Permeation Across Bionanotubes

Vikram Krishnamurthy, *Fellow, IEEE*, and Shin-Ho Chung

**Abstract**—The principles underlying Brownian dynamics (BD), its statistical consistency, and algorithms for practical implementation are outlined here. The ability to compute current flow across ion channels confers a distinct advantage to BD simulations compared to other simulation techniques. Thus, two obvious applications of BD ion channels are in calculation of the current–voltage and current–concentration curves, which can be directly compared to the physiological measurements to assess the reliability of the model and predictive power of the method. We illustrate how BD simulations are used to unravel the permeation dynamics in two biological ion channels—the KcsA K<sup>+</sup> channel and CIC Cl<sup>−</sup> channel.

**Index Terms**—Brownian dynamics (BD) simulation, interacting particles, ion channels, Langevin equation.

## I. INTRODUCTION

ALL LIVING cells are surrounded by a thin membrane, composed of two layers of phospholipid molecules, called the lipid bilayer. This thin membrane effectively partitions the external medium from the internal medium and acts as a hydrophobic, low dielectric barrier to hydrophilic molecules. The dielectric constant of the interior of the membrane is about two, whereas that of the electrolyte solutions on either side of the membrane is 80. Thus, no charged particles, such as Na<sup>+</sup>, K<sup>+</sup>, and Cl<sup>−</sup> ions, can jump across the membrane. The amount of energy needed to transport one monovalent ion, in either direction across the membrane, known as the *Born energy*, is enormously high. For a living cell to function, however, the proper ionic gradient has to be maintained, and ions at times must move across the membrane to maintain the potential difference across the membrane and to generate synaptic and action potentials. To do so, nature has devised specialized, large transmembrane protein molecules, called *ion channels*, and inserted them densely across the membrane. These ion channels form water-filled passages through which ions can freely move in and out when the gates are open. These ion channels can be viewed as biological nanotubes—although they are typically the size of angstrom units ( $10^{-10}$  m), i.e., an order of magnitude smaller in radius and length compared to carbon nanotubes that are used in nanodevices.

Manuscript received October 10, 2004; revised November 5, 2004. This work was supported in part by NSERC, in part by the Australian Research Council, and in part by the National Health and Medical Research Council of Australia.

V. Krishnamurthy is with the Department of Electrical and Computer Engineering, University of British Columbia, Vancouver, BC V6T 1Z4, Canada (e-mail: vikramk@ece.ubc.ca).

S.-H. Chung is with the Department of Theoretical Physics, Research School of Physical Sciences, Australian National University, Canberra ACT 0200, Australia (e-mail: shin-ho.chung@anu.edu.au).

Digital Object Identifier 10.1109/TNB.2004.842494

In the past few years, there have been enormous strides in our understanding of the structure–function relationships in biological ion channels. This sudden advance has been brought about by the combined efforts of experimental and computational biophysicists, who together are beginning to unravel the working principles of these exquisitely designed biological nanotubes that regulate the flow of charged particles across the living membranes. In recent breakthroughs, the crystal structures of the bacterial potassium channel, mechanosensitive channel and chloride channel have been determined from crystallographic analysis [7], [16], [17]. It is expected that crystal structures of other ion channels will follow these discoveries, ushering us into a new era in ion channel studies, where predicting function of channels from their atomic structures will become the main quest. Parallel to these landmark experimental findings, there have been also important advances in computational biophysics. As new analytical methods have been developed and the available computational power increased, theoretical models of ion permeation have become increasingly sophisticated. Now it has become possible to relate the atomic structure of an ion channel to its function through the fundamental laws of physics operating in electrolyte solutions. Many aspects of macroscopic observable properties of ion channels are being addressed by molecular and stochastic dynamics simulations. Intuitive and qualitative explanations of the permeation and selectivity of ions are beginning to be replaced by quantitative statements based on rigorous physical laws. The computational methods of solving complex biological problems, such as permeation, selectivity, and gating mechanisms of ion channels, will increasingly play prominent roles as the speed of computers increases and theoretical approaches that are currently underdevelopment become further refined.

Here we give a brief account of Brownian dynamics (BD), one of the several theoretical computational methods that are being used for treating time-dependent nonequilibrium processes that underlie the flow of currents across biological ion channels. The principles of and recent advances made by three other computational approaches—the Poisson–Nernst–Planck theory, semimicroscopic Monte Carlo method, and molecular dynamics—are detailed in the preceding and the following tutorial articles [11], [25], [37]. This paper is organized as follows. In Section II, we present a detailed discussion on the suitability of BD for modeling the permeation of ions. In Section III, a precise formulation of the BD simulation for an ion channel is given. Section IV, presents the actual BD algorithm and estimators for the ion channel current. We show that these estimators are statistically consistent. Section V describes how the BD simulation algorithm has been employed in elucidating

the mechanisms of ion permeation in the KcsA potassium channel and CIC chloride channels. Finally, in Section VI, we describe one novel extension of BD, called adaptive, controlled BD simulations.

## II. MOTIVATION FOR BD FORMULATION

The ultimate aim of theoretical biophysicists is to provide a comprehensive physical description of biological ion channels. Such a theoretical model, once successfully formulated, will link channel structure to channel function through the fundamental processes operating in electrolyte solutions. It will also concisely summarize the data, by interlacing all those seemingly unrelated and disparate observations into a connected whole. The theory will elucidate the detailed mechanisms of ion permeation—where the binding sites are in the channel, how fast an ion moves across the channel, and where the rate-limiting steps are in conduction. Finally, it will make predictions that can be confirmed or refuted experimentally.

The tools of physics employed in this endeavor, from fundamental to phenomenological, are *ab initio* and classical molecular dynamics, BD, and continuum theories. These approaches make various levels of abstractions in replacing with model the complex reality, the system composed of channel macromolecules, lipid bilayer, ions, and water molecules. One of the important criteria of successful modeling is that macroscopic observables remain invariant when the real system is replaced by the model. Each approach has the merits and demerits and is capable of providing useful information about the permeation dynamics of ion channel when applied judiciously.

At the lowest level of abstraction, we have the *ab initio* quantum mechanical approach, in which the interactions between the atoms are determined from first principles electronic structure calculations. As there are no free parameters in this approach, it represents the ultimate approach to modeling of biomolecular systems. But because of the extremely demanding nature of computations, its applications are limited to very small systems at present. A higher level of modeling abstraction is to use classical molecular dynamics [37]. Here, simulations are carried out using empirically determined pairwise interaction potentials between the atoms, and their trajectories are followed using Newton's equation of motion. Although it is possible to model an entire ion channel in this way, it is not feasible to simulate the system long enough to see permeation of ions across a model channel and to determine its conductance, which is the most important channel property.

For that purpose, one has to go up one further step in abstraction to stochastic dynamics, of which BD is the simplest form, where water molecules that form the bulk of the system in ion channels are integrated out and only the ions themselves are explicitly simulated. Thus, instead of considering the dynamics of individual water molecules, one considers their average effect as a random force or Brownian motion on the ions. This treatment of water molecules can be viewed as a functional central limit theorem approximation. In BD, it is further assumed that the protein is rigid and its dynamics is not considered. Thus, in this approach, the motion of each individual ion is modeled as

the evolution of a stochastic differential equation, known as the Langevin's equation.

A still higher level of abstraction is the Poisson–Nernst–Planck theory [11], which is based on the continuum hypothesis of electrostatics. In this and other electrodiffusion theories, one makes a further simplification, known as the mean-field approximation. Here, ions are treated not as discrete entities but as continuous charge densities that represent the space-time average of the microscopic motion of ions. In the Poisson–Nernst–Planck theory, the flux of an ionic species is described by the Nernst–Planck equation that combines Ohm's law with Fick's law of diffusion, and the potential at each position is determined from the solution of Poisson's equation using the total charge density (ions plus fixed charges). The Poisson–Nernst–Planck theory, thus, incorporates the channel structure, and its solution yields the potential, concentration, and flux of ions in the system in a self-consistent manner.

There is one other approach that has been fruitfully employed to model biological ion channels, namely, the reaction rate theory [24]. In this approach, an ion channel is represented by a series of ion binding sites separated by barriers, and ions are assumed to hop from one binding site to another, with the probability of each hop determined by the height of the energy barrier. Although the model parameters have no direct physical relation to the channel structure, many useful insights have been gleaned in the past about the mechanisms of ion permeation using this approach.

*Remark. Bionanotube Ion Channel Versus Carbon Nanotube:* There has recently been much work in the nanotechnology literature on carbon nanotubes and their use in field-effect transistors (FETs). It is worthwhile noting that our mesoscopic BD ion channel model is more complex than that of a carbon nanotube. Biological ion channels we consider here have radii of between 2 to 6 Å. In these narrow conduits formed by the protein wall, the force impinging on a permeating ion from induced surface charges on the water–protein interface becomes a significant factor. This force becomes insignificant only when the radius of the pore is more than two Debye lengths or about 16 Å for physiological salt solutions (150 mM). In comparison, carbon nanotubes used in FETs have a radius of approximately 100 Å, which is large compared to the Debye length of electrons or holes in Si. Thus the key difference is that while in carbon nanotubes point charge approximations and continuum electrostatics holds, in ion channels in general with a few exceptions the discrete finite nature of each ion needs to be taken into consideration.

## III. BD SIMULATION MODEL OF AN ION CHANNEL

### A. BD Simulation Setup

Fig. 1 illustrates the schematic setup of BD simulation for permeation of ions through an ion channel. The aim is to obtain structural information, i.e., determine channel geometry and charges in the protein that form the ion channel. An iterative approach is used as follows: First an initial estimate of the structural information of the channel, namely, the channel geometry and charges on the ionizable residues in the protein

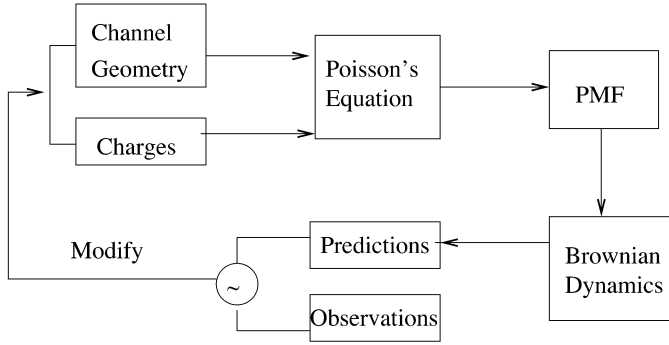


Fig. 1. BD simulation setup.

are used to determine the parameters of Poisson's equation. Numerically solving Poisson's equation yields the potential of mean profile (PMF) an ion traveling through the ion channel will experience. This in turn feeds into the BD simulation that governs the stochastic evolution of all the ions. As a result of ions modeled by BD permeating through the ion channel, a simulated ion channel current is obtained. This simulated ion channel current is compared with the experimentally observed ion channel current. The difference between the two currents is used to refine our model of the channel geometry and charges and the process repeated until the error between the simulated (predicted) ion channel current and experimentally determined ion channel current is minimized.

To carry out BD simulations of ion channels, one needs to specify the boundaries of the system. This is a relatively simple problem for one-dimensional (1-D) BD simulations [5], [23], but requires addition of reservoirs to the ion channel system in the more realistic case of three-dimensional (3-D) BD simulations [2], [8], [19].

Fig. 2 shows a schematic illustration of a BD simulation assembly for a particular example of an antibiotic ion channel called a gramicidin-A ion channel [3]. The ion channel is placed at the center of the assembly. The atoms forming the ion channel are represented as a homogeneous medium with a dielectric constant of 2 (shaded in Fig. 1). Then, a large reservoir with a fixed number of positive ions (e.g.,  $K^+$  or  $Na^+$  ions) and negative ions (e.g.,  $Cl^-$  ions) is attached at each end of the ion channel. The electrolyte in the two reservoirs comprises 55 M (moles) of  $H_2O$  and 150-mM concentrations of  $Na^+$  and  $Cl^-$  ions. The dielectric constant of the reservoirs ( $\mathcal{R}_1$  and  $\mathcal{R}_2$ ) and the interior of the ion channel  $\mathcal{C}$  is assumed to be 80. The membrane potential is imposed by applying a uniform electric field across the ion channel. This is equivalent to placing a pair of large plates far away from the ion channel and applying a potential difference between the two plates. When an ion strikes the reservoir boundary during simulations, it is elastically scattered back into the reservoir. This operation is equivalent to letting an ion enter the reservoir whenever one leaves the simulation system. Thus, the concentrations of ions in the reservoirs are maintained at the desired values at all times. During simulations of current measurements, the chosen concentration values in the reservoirs are maintained by recycling ions from one side to the other whenever there is an imbalance due to a conduction event.

The number of ions that must be placed in each reservoir for a chosen concentration depends on the size of the reservoir.

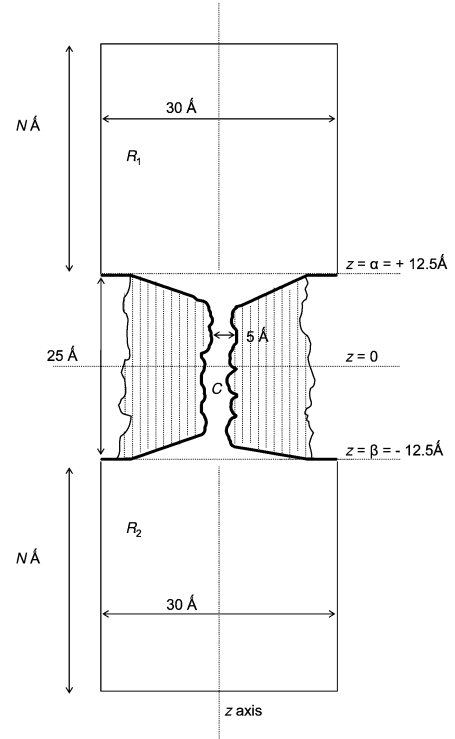


Fig. 2. Gramicidin-A ion channel model comprising  $2N$  ions within two cylindrical reservoirs  $\mathcal{R}_1$ ,  $\mathcal{R}_2$ , connected by the ion channel  $\mathcal{C}$ .

Because the computational cost is directly proportional to the number of ions in the simulation system, it is desirable to have a small reservoir. At the same time, it must be large enough such that the ions in the system are in conditions similar to those in bulk electrolyte solutions. For example, the number of ions near the entrance of the pore should fluctuate according to the binomial distribution. To meet these requirements, an elaborate treatment of boundaries using a grand canonical Monte Carlo method was proposed [22]. Subsequently, Corry *et al.* [4] showed that, provided the dimensions of the reservoirs are about three to four Debye lengths, the simple stochastic boundary as described above gives the same results as the more sophisticated method proposed by Im *et al.* [22].

### B. Permeation Model of Ion Channel

Our permeation model for the ion channel comprises two cylindrical reservoirs  $\mathcal{R}_1$  and  $\mathcal{R}_2$  connected by the ion channel  $\mathcal{C}$  as depicted in Fig. 2, in which  $2N$  ions are inserted ( $N$  denotes a positive integer). In Fig. 2, as an example we have chosen a gramicidin-A ion channel—although the results below hold for any ion channel. Throughout, we index the  $2N$  ions by  $i = 1, 2, \dots, 2N$ . These  $2N$  ions comprise the following.

- $N$  positive charged ions indexed by  $i = 1, 2, \dots, N$ . Of these,  $N/2$  ions indexed by  $i = 1, 2, \dots, N/2$  are in  $\mathcal{R}_1$  and  $N/2$  ions indexed by  $i = N/2 + 1, \dots, N$  are in  $\mathcal{R}_2$ . Each  $Na^+$  ion has charge  $q^+$ , mass  $m^{(i)} = m^+ = 3.8 \times 10^{-26}$  kg, and frictional coefficient  $m^+\gamma^+$ , and radius  $r^+$ .
- $N$  negative charge ions. We index these by  $i = N + 1, N + 2, \dots, 2N$ . Of these,  $N/2$  ions indexed by  $i = N + 1, \dots, 3N/2$  are placed in  $\mathcal{R}_1$  and the remaining  $N/2$  ions indexed by  $i = 3N/2 + 1, \dots, 2N$  are placed in  $\mathcal{R}_2$ . Each

negative ion has charge  $q^{(i)} = q^-$ , mass  $m^{(i)} = m^-$ , frictional coefficient  $m^- \gamma^-$ , and radius  $r^-$ .

Specifying the height of each reservoir to be  $N \text{ \AA}$  guarantees that the concentration of ions in them is at the physiological concentration of 150 mM.

Thus,  $\mathcal{R} = \mathcal{R}_1 \cup \mathcal{R}_2 \cup \mathcal{C}$  denotes the open set composed of the interior of the reservoirs and ion channel.

### C. Mesoscopic BD Formulation

Let  $t \geq 0$  denote continuous time. Each ion  $i$  moves in 3-D space over time. Let  $\mathbf{x}_t^{(i)} = (x_t^{(i)}, y_t^{(i)}, z_t^{(i)})' \in \mathcal{R}$  and  $\mathbf{v}_t^{(i)} \in \mathbb{R}^3$  denote the position and velocity of ion  $i$  and time  $t$ . Throughout this paper, we use  $'$  to denote transpose of a vector or matrix. The three components  $x_t^{(i)}, y_t^{(i)}, z_t^{(i)}$  of  $\mathbf{x}_t^{(i)} \in \mathcal{R}$  are, respectively, the  $x, y,$  and  $z$  position coordinates.

At time  $t = 0$ , the position  $\mathbf{x}_0^{(i)}$  and velocity  $\mathbf{v}_0^{(i)}$  of each of the  $2N$  ions indexed by  $i = 1, 2, \dots, 2N$  are randomly initialized as follows. The positive ions  $\{1, 2, \dots, N/2\}$  and negative ions  $N + 1, \dots, 3N/2$  are placed in the upper reservoir, each with  $\mathbf{x}_0^{(i)} \sim U[R_1, \Delta]$ . Similarly the remaining  $N/2$  positive ions  $\{N/2 + 1, \dots, N\}$  and remaining  $N/2$  negative ions  $\{3N/2 + 1, \dots, 2N\}$  are placed uniformly in the lower reservoir. The velocities of the  $2N$  ions are distributed according to a 3-D Gaussian distribution with zero mean, and  $3 \times 3$  diagonal positive definite covariance matrix.

An external potential  $\Phi_\lambda^{\text{ext}}(\mathbf{x})$  is applied along the  $z$  axis of Fig. 2, i.e., with  $\mathbf{x} = (x, y, z)$

$$\Phi_\lambda^{\text{ext}}(\mathbf{x}) = \lambda z, \quad \lambda \in \Lambda. \quad (1)$$

Here  $\Lambda$  denotes a finite set of applied potentials. Typically  $\Lambda = \{-200, -180, \dots, 0, \dots, 180, 200\}$  mV/m. Due to this applied external potential, the  $\text{Na}^+$  ions drift from reservoir  $\mathcal{R}_1$  to  $\mathcal{R}_2$  via the ion channel  $\mathcal{C}$  in Fig. 2.

Let  $\mathbf{X}_t = (\mathbf{x}_t^{(1)'}, \mathbf{x}_t^{(2)'}, \mathbf{x}_t^{(3)'}, \dots, \mathbf{x}_t^{(2N)'})' \in \mathcal{R}^{2N}$  denote the positions and  $\mathbf{V}_t = (\mathbf{v}_t^{(1)'}, \mathbf{v}_t^{(2)'}, \mathbf{v}_t^{(3)'}, \dots, \mathbf{v}_t^{(2N)'})' \in \mathbb{R}^{6N}$  denote the velocities of all the  $2N$  ions. The position and velocity of each individual ion evolves according to the following continuous time stochastic dynamical system:

$$\mathbf{x}_t^{(i)} = \mathbf{x}_0^{(i)} + \int_0^t \mathbf{v}_s^{(i)} ds \quad (2)$$

$$m^+ \mathbf{v}_t^{(i)} = m^+ \mathbf{v}_0^{(i)} - \int_0^t m^+ \gamma^+ \mathbf{v}_s^{(i)} ds + \int_0^t F_{,\lambda}^{(i)}(\mathbf{X}_s) ds + b^+ \mathbf{w}_t^{(i)}, \quad i \in \{1, 2, \dots, N\} \quad (3)$$

$$m^- \mathbf{v}_t^{(i)} = m^- \mathbf{v}_0^{(i)} - \int_0^t m^- \gamma^+ \mathbf{v}_s^{(i)} ds + \int_0^t F_{,\lambda}^{(i)}(\mathbf{X}_s) ds + b^- \mathbf{w}_t^{(i)}, \quad i \in \{N + 1, N + 2, \dots, 2N\}. \quad (4)$$

Equations (3) and (4) constitute the well known *Langevin* equations. The process  $\{\mathbf{w}_t^{(i)}\}$  denotes a 3-D Brownian motion,

which is component wise independent. The constants  $b^+$  and  $b^-$  are, respectively,

$$b^{+2} = 2m^+ \gamma^+ kT, \quad b^{-2} = 2m^- \gamma^- kT. \quad (5)$$

Thus, at any time  $t$ ,  $b^+ \mathbf{w}_t^{(i)}$  is a Gaussian random variable with zero mean ( $\mathbf{E}\{b^+ \mathbf{w}_t^{(i)}\} = 0$ ) and  $3 \times 3$  diagonal covariance matrix  $b^{+2} t \mathbf{I}_{3 \times 3}$ ; similarly,  $\mathbf{E}\{b^- \mathbf{w}_t^{(i)}\} = 0$  and  $\mathbf{E}\{b^- \mathbf{w}_t^{(i)}\}^2 = b^{-2} t \mathbf{I}_{3 \times 3}$ . Finally, the noise processes  $\{\mathbf{w}_t^{(i)}\}$  and  $\{\mathbf{w}_t^{(j)}\}$  that drive any two different ions  $j \neq i$  are assumed to be statistically independent.

In (3) and (4),  $F_{,\lambda}^{(i)}(\mathbf{X}_t) = -q^{(i)} \nabla_{\mathbf{x}_t^{(i)}} \Phi_{,\lambda}^{(i)}(\mathbf{X}_t)$  represents the *systematic force* acting on ion  $i$ , where the scalar valued process  $\Phi_{,\lambda}^{(i)}(\mathbf{X}_t)$  is the total electric potential experienced by ion  $i$  given the position  $\mathbf{X}_t$  of the  $2N$  ions. The subscript  $\lambda$  is the applied external potential in (1). As described below,  $F_{,\lambda}^{(i)}(\mathbf{X}_t)$  includes an ion-wall interaction force that ensures that position  $\mathbf{x}_t^{(i)}$  of each ion lies in  $\mathcal{R}$ —see (9) below.

The above system (2)–(4) can be written in stochastic differential equation form as

$$d\zeta_t = \mathbf{A} \zeta_t dt + \mathbf{f}_{,\lambda}(\zeta_t) dt + \Sigma^{1/2} d\mathbf{w}_t \quad (6)$$

where

$$\Sigma^{1/2} = \text{block diag}(\mathbf{0}_{2N \times 2N}, b^+ / m^+ \mathbf{I}_{N \times N}, b^- / m^- \mathbf{I}_{N \times N})$$

$$\mathbf{A} = \left[ \begin{array}{c|cc} \mathbf{0}_{2N \times 2N} & & \mathbf{I}_{2N \times 2N} \\ \mathbf{0}_{2N \times 2N} & -\gamma^+ \mathbf{I}_{N \times N} & \mathbf{0}_{N \times N} \\ & \mathbf{0}_{N \times N} & -\gamma^- \mathbf{I}_{N \times N} \end{array} \right] \quad (7)$$

$$\mathbf{f}_{,\lambda}(\zeta_t) = \left[ \begin{array}{c} \mathbf{0}_{2N \times 1} \\ \frac{1}{m^+} \mathbf{F}_{,\lambda}^+(\mathbf{X}_t) \\ \frac{1}{m^-} \mathbf{F}_{,\lambda}^-(\mathbf{X}_t) \end{array} \right]. \quad (8)$$

We will subsequently refer to (6) and (7) as the BD equations for the ion channel.

### D. Modeling of Systematic Force Acting on Ions

As mentioned after (4), the systematic force experienced by ion  $i$  is

$$F_{,\lambda}^{(i)}(\mathbf{X}_t) = -q^{(i)} \nabla_{\mathbf{x}_t^{(i)}} \Phi_{,\lambda}^{(i)}(\mathbf{X}_t)$$

where the scalar valued process  $\Phi_{,\lambda}^{(i)}(\mathbf{X}_t)$  denotes the total electric potential experienced by ion  $i$  given the position  $\mathbf{X}_t$  of all the  $2N$  ions. We now give a detailed formulation of these systematic forces.

The potential  $\Phi_{,\lambda}^{(i)}(\mathbf{X}_t)$  experienced by each ion  $i$  comprises the following five components:

$$\Phi_{,\lambda}^{(i)}(\mathbf{X}_t) = U(\mathbf{x}_t^{(i)}) + \Phi_\lambda^{\text{ext}}(\mathbf{x}_t^{(i)}) + \Phi^{IW}(\mathbf{x}_t^{(i)}) + \Phi^{C,i}(\mathbf{X}_t) + \Phi^{SR,i}(\mathbf{X}_t). \quad (9)$$

Just as  $\Phi_{,\lambda}^{(i)}(\mathbf{X}_t)$  is decomposed into five terms, we can similarly decompose the force  $F_{,\lambda}^{(i)}(\mathbf{X}_t) = -q\nabla_{\mathbf{x}_t^{(i)}}\Phi_{,\lambda}^{(i)}(\mathbf{X}_t)$  experienced by ion  $i$  as the superposition (vector sum) of five force terms, where each force term is due to the corresponding potential in (9)—however, for notational simplicity we describe the scalar valued potentials rather than the vector valued forces.

Note that the first three terms in (9), namely,  $U(\mathbf{x}_t^{(i)})$ ,  $\Phi_{\lambda}^{\text{ext}}(\mathbf{x}_t^{(i)})$ , and  $\Phi^{IW}(\mathbf{x}_t^{(i)})$ , depend only on the position  $\mathbf{x}_t^{(i)}$  of ion  $i$ , whereas the last two terms in (9)  $\Phi^{C,i}(\mathbf{X}_t)$  and  $\Phi^{\text{SR},i}(\mathbf{X}_t)$  depend on the distance of ion  $i$  to all the other ions, i.e., the position  $\mathbf{X}_t$  of all the ions. The five components in (9) are now defined.

- 1) PMF denoted  $U(\mathbf{x}_t^{(i)})$  in (9), comprises electric forces acting on ion  $i$  when it is in or near the ion channel (nanotube  $\mathcal{C}$  in Fig. 2). The PMF  $U$  is a smooth function of the ion position  $\mathbf{x}_t^{(i)}$  and depends on the structure of the ion channel. Therefore, estimating  $U(\cdot)$  yields structural information about the ion channel.
- 2) *External applied potential*: For ion  $i$  at position  $\mathbf{x}_t^{(i)} = \mathbf{x} = (x, y, z)$ ,  $\Phi_{\lambda}^{\text{ext}}(\mathbf{x}) = \lambda z$  [see (1)] denotes the potential on ion  $i$  due to the applied external field. The electrical field acting on each ion due to the applied potential is, therefore,  $\nabla_{\mathbf{x}_t^{(i)}}\Phi_{\lambda}^{\text{ext}}(\mathbf{x}) = (0, 0, \lambda)$  V/m at all  $\mathbf{x} \in \mathcal{R}$ . It is this applied external field that causes a drift of ions from the reservoir  $\mathcal{R}_1$  to  $\mathcal{R}_2$  via the ion channel  $\mathcal{C}$ . As a result of this drift of ions within the electrolyte in the two reservoirs, eventually the measured potential drop across the reservoirs is zero and all the potential drop occurs across the ion channel.
- 3) *Inter-ion Coulomb potential*: In (9),  $\Phi^{C,i}(\mathbf{X}_t)$  denotes the Coulomb interaction between ion  $i$  and all the other ions

$$\Phi^{C,i}(\mathbf{X}_t) = \frac{1}{4\pi\epsilon_0} \sum_{j=1, j \neq i}^{2N} \frac{q^{(j)}}{\epsilon_w \|\mathbf{x}_t^{(i)} - \mathbf{x}_t^{(j)}\|}. \quad (10)$$

- 4) *Ion-wall interaction potential*: The ion-wall potential  $\Phi^{IW}$ , also called the *Lennard–Jones potential*, ensures that the position  $\mathbf{x}_t^{(i)}$  of all ions  $i = 1, \dots, 2N$  lie in  $\mathcal{R}^o$ . With  $\mathbf{x}_t^{(i)} = (x_t^{(i)}, y_t^{(i)}, z_t^{(i)})'$ , it is modeled as

$$\Phi^{IW}(\mathbf{x}_t^{(i)}) = \frac{F_0}{9} \frac{(r^{(i)} + r_w)^{10}}{\left[ r_c + r_w - \left( \sqrt{(x_t^{(i)})^2 + (y_t^{(i)})^2} \right) \right]^9} \quad (11)$$

where for positive ions  $r^{(i)} = r^+$  (radius of  $\text{Na}^+$  atom) and for negative ions  $r^{(i)} = r^-$  (radius of  $\text{Cl}^-$  atom),  $r_w = 1.4 \text{ \AA}$  is the radius of atoms making up the wall,  $r_c$  denotes the radius of the ion channel, and  $F_0 = 2 \times 10^{-10} N$ , which is estimated from the ST2 water model used in molecular dynamics [39]. This Lennard–Jones potential results in short-range forces that are only significant when the ion is close to the wall of the reservoirs  $\mathcal{R}_1$  and  $\mathcal{R}_2$  or anywhere in the ion channel  $\mathcal{C}$  (since the ion channel is comparable in radius to the ions).

- 5) *Short-range potential*: Finally, in (9)

$$\Phi^{\text{SR},i}(\mathbf{X}_t) = \frac{F_0}{9} \sum_{j=1, j \neq i}^{2N} \frac{(r^{(i)} + r^{(j)})}{\|\mathbf{x}_t^{(i)} - \mathbf{x}_t^{(j)}\|^9} \quad (12)$$

denotes the short-range Coulomb interaction between two ions when their electron clouds overlap. Similar to the Lennard–Jones potential,  $\Phi^{\text{SR},i}$  is significant only when ion  $i$  gets very close to another ion. It ensures that two opposite charge ions attracted by inter-ion Coulomb forces (10) cannot collide and annihilate each other.

*Remark*: As discussed previously, the above BD approach does not explicitly model the water molecules the surround an ion. Instead the average effect of the water molecules is considered as two terms in (3) and (4).

- 1) The friction term  $m\gamma\mathbf{v}_t^{(i)}dt$  captures the average effect of the ions driven by the applied external electrical field bumping into the water molecules every few femtoseconds. The frictional coefficient is given from Einstein's relation.
- 2) The Brownian motion term  $\mathbf{w}_t^{(i)}$  also captures the effect of the random motion of ions bumping into water molecules and is given from the *fluctuation–dissipation* theorem.

#### IV. STATISTICAL CONSISTENCY OF BD SIMULATIONS FOR ION CHANNEL CURRENTS

Assume that the system (6) comprising  $2N$  ions has attained stationarity with the ion channel  $\mathcal{C}$  closed. It can be proved [27] that the system (6) is exponentially ergodic and converges to its stationary distribution geometrically fast. Then the ion channel is opened so that ions can diffuse into it. Let  $\tau_{\mathcal{R}_1, \mathcal{R}_2}^{(\cdot, \lambda)}$  denote the mean minimum time for any of the  $N/2$   $\text{Na}^+$  ions in  $\mathcal{R}_1$  to travel to  $\mathcal{R}_2$  via the ion channel  $\mathcal{C}$ , and  $\tau_{\mathcal{R}_2, \mathcal{R}_1}^{(\cdot, \lambda)}$  denote the minimum time for any of the  $N/2$   $\text{Na}^+$  ions in  $\mathcal{R}_2$  to travel to  $\mathcal{R}_1$ :  $\tau_{\mathcal{R}_1, \mathcal{R}_2}^{(\cdot, \lambda)} = \mathbf{E}\{t_{\beta}\}$  and  $\tau_{\mathcal{R}_2, \mathcal{R}_1}^{(\cdot, \lambda)} = \mathbf{E}\{t_{\alpha}\}$ , where

$$t_{\beta} \triangleq \inf \left\{ t : \max \left( z_t^{(1)}, z_t^{(2)}, \dots, z_t^{(N/2)} \right) \geq \beta \right\}$$

$$t_{\alpha} \triangleq \inf \left\{ t : \min \left( z_t^{(N/2+1)}, z_t^{(N/2+2)}, \dots, z_t^{(2N)} \right) \leq \alpha \right\}. \quad (13)$$

It can be shown that  $\tau_{\mathcal{R}_1, \mathcal{R}_2}^{(\cdot, \lambda)}$  and  $\tau_{\mathcal{R}_2, \mathcal{R}_1}^{(\cdot, \lambda)}$  satisfy a boundary valued partial differential equation. In terms of the mean first passage times  $\tau_{\mathcal{R}_1, \mathcal{R}_2}^{(\cdot, \lambda)}$ ,  $\tau_{\mathcal{R}_2, \mathcal{R}_1}^{(\cdot, \lambda)}$  defined in (13), the mean current flowing from  $\mathcal{R}_1$  via the ion channel  $\mathcal{C}$  into  $\mathcal{R}_2$  is defined as

$$I(\lambda) = q^+ \left( \frac{1}{\tau_{\mathcal{R}_1, \mathcal{R}_2}^{(\cdot, \lambda)}} - \frac{1}{\tau_{\mathcal{R}_2, \mathcal{R}_1}^{(\cdot, \lambda)}} \right). \quad (14)$$

However, it is not possible to obtain explicit closed form expressions for the mean first passage times  $\tau_{\mathcal{R}_2, \mathcal{R}_1}^{(\cdot, \lambda)}$  and  $\tau_{\mathcal{R}_1, \mathcal{R}_2}^{(\cdot, \lambda)}$  and, hence, the current  $I(\cdot)$  in (14). The aim of BD simulation is to obtain estimates of these quantities by directly simulating the stochastic dynamical system (6). In this section, we show that the current estimates  $\hat{I}_L(\lambda)$  (defined below) obtained

from a  $L$ -iteration BD simulation are statistically consistent, i.e.,  $\lim_{L \rightarrow \infty} \hat{I}_L(\lambda) = I(\lambda)$  a.s.

Due to the applied external potential  $\Phi_\lambda^{\text{ext}}$  [see (9)], ions drift from reservoir  $\mathcal{R}_1$  via the ion channel  $\mathcal{C}$  to the reservoir  $\mathcal{R}_2$ , thus generating an ion channel current. In order to construct an estimate for the current flowing from  $\mathcal{R}_1$  to  $\mathcal{R}_2$  in the BD simulation, we need to count the number of up-crossings of ions (i.e., the number of times ions cross from  $\mathcal{R}_1$  to  $\mathcal{R}_2$  across the region  $\mathcal{C}$ ) and down-crossings (i.e., the number of times ions cross from  $\mathcal{R}_2$  to  $\mathcal{R}_1$  across the region  $\mathcal{C}$ ). Recall from Fig. 2 that  $z = \alpha = -12.5 \text{ \AA}$  denotes the boundary between  $\mathcal{R}_1$  and  $\mathcal{C}$ , and  $z = \beta = 12.5 \text{ \AA}$  denotes the boundary between  $\mathcal{R}_2$  and  $\mathcal{C}$ .

*Time Discretization:* The BD simulation Algorithm 1 described below propagates the  $2N$  ions over a period of  $T = 10^{-4}$  seconds according to a time discretization of (6). Consider a regular partition  $0 = t_0 < t_1 < \dots < t_{k-1} < t_k < \dots$  with constant time step  $\Delta = t_k - t_{k-1} = 10^{-15}$  (femto) seconds. There are several possible methods for discretizing a stochastic differential equation; see [26] for a detailed exposition. Here we adopt the method of [20] which can be straightforwardly explained as follows: assuming  $\mathbf{f}_{i,\lambda}(\zeta_t)$  to be approximately constant over the short time interval  $[t_k, t_{k+1}]$ , the solution of (6) satisfies

$$\zeta_{t_{k+1}} = e^{\mathbf{A}(t_{k+1}-t_k)} \zeta_{t_k} + \int_{t_k}^{t_{k+1}} e^{\mathbf{A}(t_{k+1}-\tau)} \mathbf{f}_{i,\lambda}(\zeta_{t_k}) d\tau + \int_{t_k}^{t_{k+1}} e^{\mathbf{A}(t_{k+1}-\tau)} \Sigma^{1/2} d\mathbf{w}_\tau. \quad (15)$$

The last integral above is merely a Gauss–Markov process. For notational convenience, we denote the above discretized system as the following discrete-time system with  $k = 0, 1, \dots$  denoting discrete-time

$$\zeta_{k+1}^{(d)} = \Gamma \zeta_k^{(d)} + \mathbf{f}_{i,\lambda}(\zeta_k^{(d)}) + \mathbf{w}_k^{(d)}. \quad (16)$$

Here  $k$  corresponds to time  $t_k$ ,  $\{\zeta_k^{(d)}\}$  denotes the discrete-time state, and  $\Gamma = \exp(\mathbf{A}\Delta)$ ,  $\mathbf{w}_k^{(d)}$  is a discrete-time vector Gauss–Markov process.

*BD Simulation Algorithm:* In the BD simulation Algorithm 1 below, we use the following notation:

The algorithm runs for  $L$  iterations where  $L$  is user specified. Each iteration  $l$ ,  $l = 1, 2, \dots, L$  runs for a random number of discrete-time steps until an ion crosses the channel. We denote these random times as  $\hat{\tau}_{\mathcal{R}_1, \mathcal{R}_2}^{(l)}$  if the ion has crossed from  $\mathcal{R}_1$  to  $\mathcal{R}_2$  and  $\hat{\tau}_{\mathcal{R}_2, \mathcal{R}_1}^{(l)}$  if the ion has crossed from  $\mathcal{R}_2$  to  $\mathcal{R}_1$ . Thus

$$\hat{\tau}_{\mathcal{R}_1, \mathcal{R}_2}^{(l)} = \min \left\{ k : \zeta_k^{(d)} \in \mathcal{Pr} \right\}$$

$$\hat{\tau}_{\mathcal{R}_2, \mathcal{R}_1}^{(l)} = \min \left\{ k : \zeta_k^{(d)} \in \mathcal{P}_1 \right\}.$$

The positive ions  $\{1, 2, \dots, N/2\}$  are in  $\mathcal{R}_1$  at steady state  $\pi_\infty^{(\lambda)}$ , and the positive ions  $\{N/2 + 1, \dots, 2N\}$  are in  $\mathcal{R}_2$  at steady state.

$L_{\mathcal{R}_1, \mathcal{R}_2}$  is a counter that counts how many  $\text{Na}^+$  ions have crossed from  $\mathcal{R}_1$  to  $\mathcal{R}_2$  and  $L_{\mathcal{R}_2, \mathcal{R}_1}$  counts how many  $\text{Na}^+$  ions have crossed from  $\mathcal{R}_2$  to  $\mathcal{R}_1$ . Note  $L_{\mathcal{R}_1, \mathcal{R}_2} + L_{\mathcal{R}_2, \mathcal{R}_1} = L$ .

In the algorithm below, to simplify notation we only consider passage of positive  $\text{Na}^+$  ions  $i = 1, \dots, N$  across the

ion channel (for example, in a gramicidin-A channel, the ion channel current is caused only by  $\text{Na}^+$  ions).

**Algorithm 1: Brownian Dynamics Simulation Algorithm (for fixed  $\lambda$ )**

- Input parameters for PMF and  $\lambda$  for applied external potential.
- For  $l = 1$  to  $L$  iterations:
  - *Step 1.* Initialize all  $2N$  ions according to stationary distribution  $\pi_\infty^{(\lambda)}$ .  
Open ion channel at discrete time  $k = 0$  and set  $k = 1$ .
  - *Step 2.* Propagate all  $2N$  ions according to the time discretized Brownian dynamical system (16) until time  $k^*$  at which an ion crosses the channel.
    - \* If ion crossed ion channel from  $\mathcal{R}_1$  to  $\mathcal{R}_2$ , i.e., for any ion  $i^* \in \{1, 2, \dots, N/2\}$ ,  $z_{k^*}^{(i^*)} \geq \beta$  then set  $\hat{\tau}_{\mathcal{R}_1, \mathcal{R}_2}^{(l)} = k^*$ .  
Update number of crossings from  $\mathcal{R}_1$  to  $\mathcal{R}_2$ :  
 $L_{\mathcal{R}_1, \mathcal{R}_2} = L_{\mathcal{R}_1, \mathcal{R}_2} + 1$ .
    - \* If ion crossed ion channel from  $\mathcal{R}_2$  to  $\mathcal{R}_1$ , i.e., for any ion  $i^* \in \{N/2 + 1, \dots, N\}$ ,  $z_{k^*}^{(i^*)} \leq \alpha$  then set  $\hat{\tau}_{\mathcal{R}_2, \mathcal{R}_1}^{(l)} = k^*$ .  
Update number of crossings from  $\mathcal{R}_2$  to  $\mathcal{R}_1$ :  
 $L_{\mathcal{R}_2, \mathcal{R}_1} = L_{\mathcal{R}_2, \mathcal{R}_1} + 1$ .
  - End for loop.
- Compute the mean first passage time and mean current estimate after  $L$  iterations as

$$\hat{\tau}_{\mathcal{R}_1, \mathcal{R}_2}^{(\lambda)}(L) = \frac{1}{L_{\mathcal{R}_1, \mathcal{R}_2}} \sum_{i=1}^{L_{\mathcal{R}_1, \mathcal{R}_2}} \hat{\tau}_{\mathcal{R}_1, \mathcal{R}_2}^{(i)} \quad (17)$$

$$\hat{\tau}_{\mathcal{R}_2, \mathcal{R}_1}^{(\lambda)}(L) = \frac{1}{L_{\mathcal{R}_2, \mathcal{R}_1}} \sum_{i=1}^{L_{\mathcal{R}_2, \mathcal{R}_1}} \hat{\tau}_{\mathcal{R}_2, \mathcal{R}_1}^{(i)} \quad (18)$$

$$\hat{I}_L(\lambda) = q^+ \left( \frac{1}{\hat{\tau}_{\mathcal{R}_1, \mathcal{R}_2}^{(\lambda)}(L)} - \frac{1}{\hat{\tau}_{\mathcal{R}_2, \mathcal{R}_1}^{(\lambda)}(L)} \right). \quad (19)$$

The following result shows that the estimated current  $\hat{I}_L(\lambda)$  obtained from a BD simulation run over  $L$  iterations is strongly consistent.

*Theorem 1:* For applied external potential  $\lambda \in \Lambda$ , the ion channel current estimate  $\hat{I}_L(\lambda)$  obtained from the BD simulation Algorithm 1 over  $L$  iterations is strongly consistent, i.e.,

$$\lim_{L \rightarrow \infty} \hat{I}_L(\lambda) = I(\lambda) \quad \text{w.p. 1} \quad (20)$$

where  $I(\lambda)$  is the mean current defined in (14).

*Proof:* Since by construction in Algorithm 1, each of the  $L$  iterations are statistically independent, and  $\mathbf{E} \left\{ \hat{\tau}_{\mathcal{R}_1, \mathcal{R}_2}^{(l)} \right\}$ ,  $\mathbf{E} \left\{ \hat{\tau}_{\mathcal{R}_2, \mathcal{R}_1}^{(l)} \right\}$  are finite by Kolmogorov's strong law of large numbers

$$\lim_{L \rightarrow \infty} \hat{\tau}_{\mathcal{R}_1, \mathcal{R}_2}^{(\lambda)}(L) = \tau_{\mathcal{R}_1, \mathcal{R}_2}^{(\lambda)}$$

$$\lim_{L \rightarrow \infty} \hat{\tau}_{\mathcal{R}_2, \mathcal{R}_1}^{(\lambda)}(L) = \tau_{\mathcal{R}_2, \mathcal{R}_1}^{(\lambda)} \quad \text{w.p. 1.}$$

Thus,  $q^+ \left( \left( 1/\hat{\tau}_{\mathcal{R}_1, \mathcal{R}_2}^{(\lambda)}(L) \right) - \left( 1/\hat{\tau}_{\mathcal{R}_2, \mathcal{R}_1}^{(\lambda)}(L) \right) \right) \rightarrow I(\lambda)$  w.p. 1 as  $L \rightarrow \infty$ .  $\blacksquare$

## V. BD STUDIES ON ION CHANNELS

Here we highlight some of the computational studies carried out on two important classes of biological ion channels—the KcsA potassium channel and CIC Cl<sup>-</sup> channel. In the absence of structural information for biological ion channels, the gramicidin pore has been the main focus of theoretical investigations for a long time [3]. The recent determinations of the crystal structures of several biological ion channels [16], [17], [18], [41] have now shifted the attention away from the gramicidin channel. For detailed accounts of recent advances in the field of computational biophysics, the reader is referred to several review articles [10], [28], [36], [40].

### A. KcsA Potassium Channel

The unraveling of the crystal structure of the KcsA potassium channel by Doyle *et al.* [16] is a landmark event that will have a lasting impact on ion channel studies. This is the first biological ion channel whose X-ray structure is elucidated. Thus, it has prompted a flurry of theoretical investigations on the mechanisms underlying the permeation of ions across the channel, the basis of ion selectivity, and the conformational changes that occur in the KcsA protein when the channel opens.

To determine currents flowing across the channel, Chung *et al.* [8], [9] and others [6], [30] have performed BD simulations on the KcsA channel using the experimentally determined channel structure. In these simulations, water is treated implicitly as a continuum, and the protein atoms forming the channel are assumed to be rigid. With these simplifications, they were able to relate the channel function to its structure.

The shape of the ion-conducting pathway across the KcsA protein is illustrated in the inset of Fig. 3. The KcsA structure determined from X-ray diffraction consists of 396 amino acid residues, or 3504 atoms excluding polar hydrogens. The channel is constructed by four subunits of a tetramer of peptide chains, each subunit consisting of an outer helix, inner helix, pore helix and a threonine-valine-glycine-tyrosine-glycine (TVGYG) amino acid sequence that forms the selectivity filter. The protein atoms form a central pore between these subunits. An outline of the pore reveals that the channel is composed of three segments—a long intracellular region of length 20 Å lined with hydrophobic amino acids extending toward the intracellular space (left-hand side in the inset), a wide water-filled chamber of length 10 Å, and a narrow selectivity filter of length 12 Å, extending toward the extracellular space. The selectivity filter is the most important element in this structure as it can distinguish K<sup>+</sup> ions from those of Na<sup>+</sup> on the basis of their sizes (crystal radius of K<sup>+</sup> is 1.33 Å and that of Na<sup>+</sup> is 0.95 Å). BD simulations show that there are three regions in the selectivity filter and cavity where K<sup>+</sup> ions dwell preferentially, as illustrated in the inset of Fig. 3 (indicated as dark balls). There is also another prominent binding site near the intracellular entrance of the channel. The preferred position where ions dwell preferentially are in close agreement with the positions observed in Rb<sup>+</sup> X-ray diffraction maps [16].

To illustrate the permeation mechanism across the potassium channel, the channel is bisected such that ions in the chamber and filter are consigned to the right side, and the rest to the

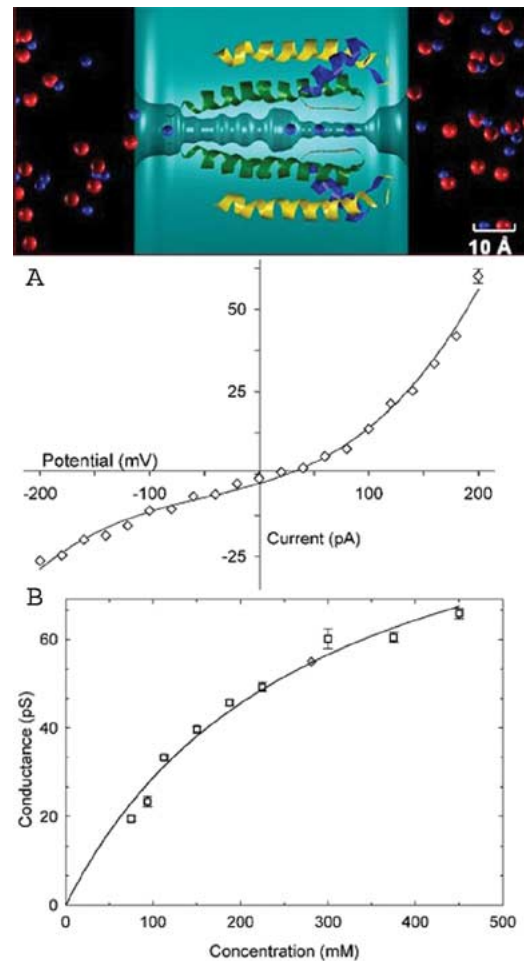


Fig. 3. KcsA potassium ion channel: shape of ion channel, current voltage, and current concentration curves.

left side. The most common situation in the conducting state of the channel has one ion on the left half, and two ions in the right half. This configuration is referred to as the [1, 2] state. A typical conduction event consists of the following transitions: [1, 2] → [0, 3] → [0, 2] → [1, 2]. In other words, the ion waiting near the intracellular mouth overcomes a small energy barrier in the intracellular pore to enter the chamber region. Because this system is unstable in the presence of an applied potential, the rightmost ion is ejected from the channel. Another ion enters the intracellular mouth, leaving the system in its original configuration. The precise sequence of events taking place for conduction of ions depends on their concentration, applied potential, and the ionization state of charged residues at the intracellular gate, and many other states can be involved in the conduction process depending on the values of these variables.

In Fig. 3(a) and (b), we show the current–voltage and current–concentration curves obtained from BD simulations [9]. The results of BD simulations are in broad agreement with those determined experimentally [13], [15], [21], [29], [31], [38]. The conductances at +150 mV and –150 mV are, respectively,  $172 \pm 15$  and  $93 \pm 12$  pS. The relationship is linear when the applied potential is in the physiological range but deviates from Ohm's law at a higher applied potential, especially at high positive potentials. The current saturates with an increasing ionic concentrations, as shown in Fig. 3(b). This

arises because ion permeation across the channel is governed by two independent processes: the time it takes for an ion to enter the channel mouth depends on the concentration while the time it takes for the ion to reach the oval chamber is independent of the concentration but depends solely on the applied potential.

BD studies reveal that permeation across the filter is much faster than in other parts of the channel. That is, once a third ion reaches the oval cavity, the outermost ion in the selectivity filter is expelled almost instantaneously. Thus, although the filter plays a crucial role in selecting the  $K^+$  ions, its role in influencing their conductance properties is minimal.

### B. CLC $Cl^-$ Channel

Dutzler *et al.* [17], [18] determined the X-ray structure of a transmembrane protein in bacteria, known as the CIC channel, that has subsequently been shown to be a transporter, not an ion channel [1]. Nevertheless, many amino acid sequences of the bacterial CIC protein are conserved in their eukaryotic CIC relatives, which are selectively permeable to  $Cl^-$  ions. The prototype channel, known as CIC-0, first discovered and characterized by Miller [32], is found in *Torpedo electroplax*. Since then, nine different human CIC genes and four plant and bacterial CIC genes have been identified. The CIC family of  $Cl^-$  channel is present in virtually all tissues—in muscle, heart, brain, kidney, and liver—and is widely expressed in most mammalian cells. By allowing  $Cl^-$  ions to cross the membrane, CIC channels perform diverse physiological roles, such as control of cellular excitability, cell volume regulation, and regulation of intracellular pH [35].

The availability of the X-ray structure of the bacterial CIC  $Cl^-$  channel has prompted several theoretical investigations using a novel computational approach based on the Metropolis Monte Carlo method [33], molecular dynamics, [12] and BD [14]. Because the bacterial CIC protein shares many signature sequence identities with the eukaryotic CIC channels, it is possible to build homology models of these channels based on the structural information provided by Dutzler *et al.* [17], [18]. With this aim in mind, Corry *et al.* [14] first altered the X-ray structure of the bacterial CIC protein using molecular dynamics to create an open-state configuration. They then converted the bacterial CIC structure to the CIC-0 structure (see, for details, [14]). Incorporating this homology model into BD, as shown in the inset of Fig. 4, they determined the current–voltage–concentration profile of CIC-0. These are illustrated in Fig. 4(a) and (b). The current–voltage relationship determined from BD simulations is linear (filled circles in Fig. 4(a)), with the slope conductance of  $11.3 \pm 0.5$  pS. The experimental measurements obtained from CIC-0 [32] (open circles) are superimposed on the simulated data. The slope conductance determined from the experimental data is  $9.4 \pm 0.1$  pS. In Fig. 4(b), the currents obtained from BD simulations, under the applied potential of  $-80$  mV, are plotted against the concentration of  $Cl^-$  ions in the reservoirs. The experimental data obtained from CIC-0 by T.-Y. Chen (personal communication) are shown in open circles. The lines fitted through the data points are calculated from the Michaelis–Menten equation. There is a reasonable agreement between the simulated data and experimental measurements for CIC-0.

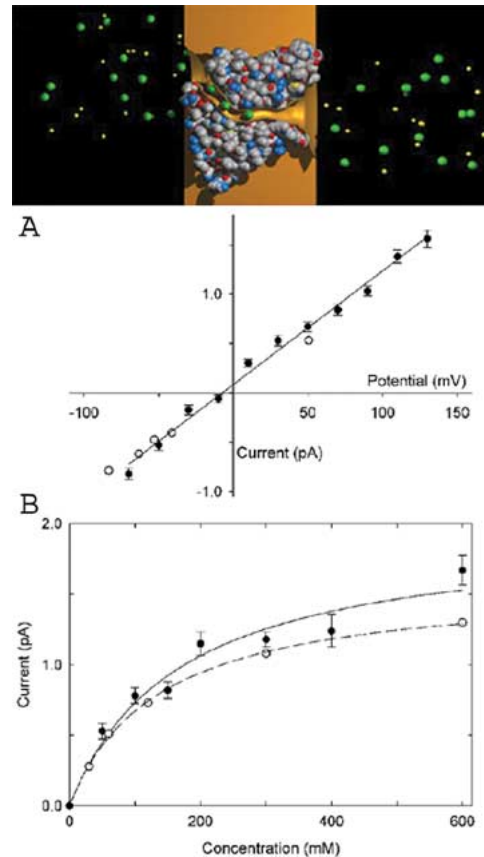


Fig. 4. CIC  $Cl^-$  channel ion channel: shape of ion channel, current–voltage, and current–concentration curves.

BD simulations also reveal the steps involved in permeation of  $Cl^-$  ions across the CIC channel. The pore is normally occupied by two  $Cl^-$  ions. When a third ion enters the pore from the intracellular space (left-hand side in the inset of Fig. 4), the stable equilibrium is disrupted, and the outermost  $Cl^-$  ion is expelled to the extracellular space.

## VI. CONTROLLED BD FOR PMF ESTIMATION

In this section, we briefly describe a new extension of BD simulation for estimating the PMF of an ion channel. This extension involves a novel simulation-based learning control algorithm that dynamically adapts the evolution of the BD simulation. It is based on our current and ongoing research. The complete formalism, convergence proofs, and numerical results will be presented elsewhere [27].

We will estimate the PMF  $U_\theta$  parameterized by some finite dimensional parameter  $\theta$  (e.g.,  $\theta$  are the means variances and mixture weights of a Gaussian basis function approximation), by computing the parameter  $\theta$  that optimizes the fit between the mean current  $I(\theta, \lambda)$  [defined above in (14)] and the experimentally observed current  $y(\lambda)$  defined below. There are two reasons why estimating the PMF  $U_\theta$  is useful. First, it allows us to determine the position and depth of the potential wells and barriers in the ion channel. Second, estimating the PMF permits us to compute the effective surface charge density along the protein of the inside surface of the ion channel that reproduces the PMF  $U_\theta$  along the central  $z$  axis of the ion channel; see [27] for details.

Unfortunately, it is impossible to explicitly compute  $I(\theta, \lambda)$  from (14). For this reason we resort to a *stochastic optimization problem formulation* below, where consistent estimates of  $I(\theta, \lambda)$  are obtained via the BD simulation Algorithm 1.

From patch clamp experimental data, an accurate estimate of the  $I$ - $V$  curve of an ion channel can be obtained. This  $I$ - $V$  curve depicts the the actual current  $y(\lambda)$  flowing through an ion channel for various external applied potentials  $\lambda \in \Lambda$ . For fixed applied field  $\lambda \in \Lambda$ , define the square error loss function between the mathematically defined mean current  $I(\theta, \lambda)$  in (14) and the true current  $y(\lambda)$  as

$$Q(\theta, \lambda) = |I(\theta, \lambda) - y(\lambda)|^2. \quad (21)$$

Define the total loss function obtained by adding the square error over all the applied fields  $\lambda \in \Lambda$  on the  $I$ - $V$  curve as

$$Q(\theta) = \sum_{\lambda \in \Lambda} Q(\theta, \lambda). \quad (22)$$

The optimal PMF  $U_{\theta^*}$  is determined by the parameter  $\theta^*$  that best fits the mean current  $I(\theta, \lambda)$  to the experimentally determined  $I$ - $V$  curve of an ion channel, i.e.,

$$\theta^* = \arg \min_{\theta \in \Theta} Q(\theta). \quad (23)$$

However, the deterministic optimization (21) and (23) cannot be directly carried out, since it is not possible to obtain explicit closed form expressions for the current  $I(\theta, \lambda)$  in (21). This motivates us to formulate the estimation of the PMF as a stochastic optimization problem where  $I(\theta, \lambda)$  is replaced by estimates from the BD simulation.

Suppose that the BD simulation Algorithm 1 is run in batches indexed by batch number  $n = 1, 2, \dots$ . In each batch  $n$ , the PMF parameter  $\theta_n$  is selected (as described below), the BD Algorithm 1 is run over  $L$  iterations, and the estimated current  $\hat{I}_n(\theta, \lambda)$  is computed using (19). Since as proved in Theorem 1 these estimates are asymptotically unbiased, i.e.,  $\mathbf{E} \left\{ \hat{I}_n(\theta, \lambda) \right\} = I(\theta, \lambda)$ , we can reexpress the objective function  $Q(\theta, \lambda) = |I(\theta, \lambda) - y(\lambda)|^2$  in (21) as

$$Q(\theta, \lambda) = \left( \mathbf{E} \left\{ \hat{I}_n(\theta, \lambda) \right\} - y(\lambda) \right)^2, \quad Q(\theta) = \sum_{\lambda \in \Lambda} Q(\theta, \lambda). \quad (24)$$

To summarize, (23) and (24) defines the stochastic optimization problem we will solve in this section.

To solve the stochastic optimization problem by a simulation based optimization approach, we need to evaluate unbiased estimates  $Q_n(\theta, \lambda)$  of the loss function and derivative estimates  $\hat{\nabla}_{\theta} Q_n(\theta, \lambda)$ . The estimation of the derivative  $\hat{\nabla}_{\theta} Q_n(\theta, \lambda)$  involves using recent sophisticated techniques in Monte Carlo gradient estimation [34]. In [27] we present several such algorithms, including the Kiefer-Wolfowitz algorithm, which evaluates derivate estimates as finite differences, the Simultaneous Perturbation Stochastic Approximation (SPSA), which evaluates the derivatives in random directions (and, thus, saves computational cost), and pathwise infinitesimal perturbation analysis (IPA) gradient estimators.

The controlled BD simulation algorithm for estimating the PMF is schematically depicted in Fig. 5. Recall  $n = 0, 1, \dots$  denotes batch number.

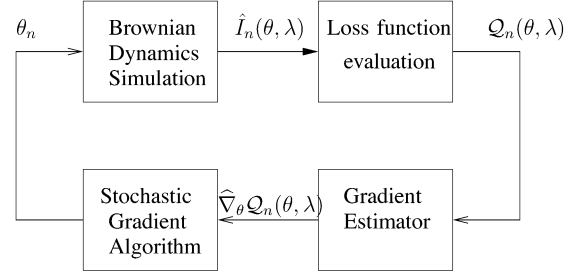


Fig. 5. Controlled BD simulation for estimation PMF.

**Algorithm 2: Controlled BD Simulation Algorithm for estimating PMF**

- *Step 0* (Set batch index  $n = 0$ , and initialize  $\theta_0 \in \Theta$ ).
- *Step 1* (Evaluation of loss function): At batch  $n$ , evaluate loss function  $Q_n(\theta, \lambda)$  for each external potential  $\lambda \in \Lambda$ .
- *Step 2* (Gradient Estimation): Compute gradient estimate  $\hat{\nabla}_{\theta} Q_n(\theta, \lambda)$ .
- *Step 3* (Stochastic Approximation Algorithm): Update PMF estimate:

$$\theta_{n+1} = \theta_n - \epsilon_{n+1} \sum_{\lambda \in \Lambda} \hat{\nabla}_{\theta} Q_n(\theta_n, \lambda) \quad (25)$$

where  $\epsilon_n = 1/n$  denotes a decreasing step size.

- Set  $n$  to  $n + 1$  and go to Step 1.

A crucial aspect of the above algorithm is the gradient estimation Step 2. In this step, an estimate  $\hat{\nabla}_{\theta} Q_n(\theta, \lambda)$  of the gradient  $\nabla_{\theta} Q_n(\theta, \lambda)$  is computed. This gradient estimate is then fed to the stochastic gradient algorithm (Step 3), which updates the PMF.

It is proved in [27] that the above algorithm converges with probability one to the optimal PMF  $\theta^*$ .

## REFERENCES

- [1] A. Accardi and C. Miller, "Secondary active transport mediated by a prokaryotic homologue of CIC Cl<sup>-</sup> channels," *Nature*, vol. 427, pp. 803–807, 2004.
- [2] T. W. Allen and S. H. Chung, "Brownian dynamics study of an open-state KcsA potassium channel," *Biochim. Biophys. Acta—Biomembrane*, vol. 1515, pp. 83–91, 2001.
- [3] O. S. Andersen, R. Koepell, and B. Roux, *IEEE Trans. Nanobiosci.*, vol. 4, no. 1, Mar. 2005.
- [4] B. Corry *et al.*, "Reservoir boundaries in Brownian dynamics simulations of ion channels," *Biophys. J.*, vol. 82, pp. 1975–1984, Apr. 2002.
- [5] S. Bek and E. Jakobsson, "Brownian dynamics study of a multiply occupied cation channel: Application to understanding permeation in potassium channel," *Biophys. J.*, vol. 66, pp. 1028–1038, 1994.
- [6] A. Burykin, C. N. Schutz, J. Villa, and A. Warshel, "Simulations of ion current realistic models of ion channels: KcsA potassium channel," *Proteins*, vol. 47, pp. 265–280, 2002.
- [7] G. Chang, R. H. Spencer, A. T. Lee, M. T. Barclay, and D. C. Rees, "Structure of the mscl homolog from mycobacterium tuberculosis: A gated mechanosensitive channel," *Science*, vol. 282, pp. 2220–2226, 1998.
- [8] S. H. Chung, T. W. Allen, M. Hoyles, and S. Kuyucak, "Permeation of ions across the potassium channel: Brownian dynamics studies," *Biophys. J.*, vol. 77, pp. 2517–2533, 1999.
- [9] S. H. Chung, T. W. Allen, and S. Kuyucak, "Conducting-state properties of the KcsA potassium channel from molecular and Brownian dynamics simulations," *Biophys. J.*, vol. 82, pp. 628–645, 2002.
- [10] S. H. Chung and S. Kuyucak, "Recent advances in ion channel research," *Biochim. Biophys. Acta*, vol. 1565, pp. 267–286, 2002.

- [11] R. D. Coalson, "Poisson–Nernst–Planck theory approach to the calculation of current through biological ion channels," *IEEE Trans. Nanobiosci.*, vol. 4, no. 1, pp. 81–93, Mar. 2005.
- [12] J. Cohen and K. Schulten, "Mechanism of anionic conduction across CIC," *Biophys. J.*, vol. 86, pp. 836–845, 2004.
- [13] R. Coronado, R. L. Rosenberg, and C. Miller, "Tonic selectivity, saturation, and block in a  $K^+$ -selective channel from sarcoplasmic reticulum," *J. Gen. Physiol.*, vol. 76, pp. 425–446, 1980.
- [14] B. Corry, M. O'Mara, and S. H. Chung, "Conduction mechanisms of chloride ions in CIC-type channels," *Biophys. J.*, vol. 86, pp. 846–860, 2004.
- [15] L. G. Cuello, J. G. Romero, D. M. Cortes, and E. Perozo, "pH dependent gating in the streptomyces lividans  $K^+$  channel," *Biochemistry*, vol. 37, pp. 3229–3236, 1998.
- [16] D. A. Doyle, J. M. Cabral, R. A. Pfuetzner, A. Kuo, J. M. Gulbis, S. L. Cohen, B. T. Chait, and R. MacKinnon, "The structure of the potassium channel: Molecular basis of  $K^+$  conduction and selectivity," *Science*, vol. 280, pp. 69–77, 1998.
- [17] R. Dutzler, E. B. Campbell, M. Cadene, B. T. Chait, and R. MacKinnon, "X-ray structure of a CIC chloride channel at 3.0 Å reveals the molecular basis of anion selectivity," *Nature*, vol. 415, pp. 287–294, 2002.
- [18] R. Dutzler, E. B. Campbell, and R. MacKinnon, "Gating the selectivity in CIC chloride channels," *Science*, vol. 300, pp. 108–112, 2003.
- [19] S. Edwards, B. Corry, S. Kuyucak, and S. H. Chung, "Continuum electrostatics fails to describe ion permeation in the gramicidin channel," *Biophys. J.*, vol. 83, pp. 1348–1360, Sep. 2002.
- [20] W. F. van Gunsteren, H. J. Berendsen, and J. A. C. Rullmann, "Stochastic dynamics for molecules with constraints Brownian dynamics of n-alkalines," *Mol. Phys.*, vol. 44, no. 1, pp. 69–95, 1981.
- [21] L. Heginbotham, M. LeMasurier, L. Kolmakova-Partensky, and C. Miller, "Single streptomyces lividans  $K^+$  channels: Functional asymmetries and sidedness of proton activation," *J. Gen. Physiol.*, vol. 114, pp. 551–559, 1999.
- [22] W. Im, S. Seefeld, and B. Roux, "A grand canonical Monte Carlo-Brownian dynamics algorithm for simulating ion channels," *Biophys. J.*, vol. 79, pp. 788–801, 2000.
- [23] E. Jakobsson and S. W. Chiu, "Stochastic theory of ion movement in channels with single-ion occupancy. application to sodium permeation of Gramicidin channels," *Biophys. J.*, vol. 52, pp. 33–45, 1987.
- [24] P. C. Jordan, "Fifty years of progress in ion channel research," *IEEE Trans. Nanobiosci.*, vol. 4, no. 1, pp. 1–9, Mar. 2005.
- [25] ———, "Semimicroscopic modeling of permeation through ion channels," *IEEE Trans. Nanobiosci.*, vol. 4, no. 1, pp. 94–101, Mar. 2005.
- [26] P. E. Kloeden and E. Platen, *Numerical Solution of Stochastic Differential Equations*. Berlin, Germany: Springer-Verlag, 1992.
- [27] V. Krishnamurthy and S. H. Chung, "Exact formulation of adaptive controlled Brownian dynamics for studying the permeation dynamics in ion channels," to be published.
- [28] S. Kuyucak, O. S. Andersen, and S. H. Chung, "Models of permeation in ion channels," in *Rep. Prog. Phys.*, 2001, vol. 64, pp. 1427–1472.
- [29] M. LeMasurier, L. Heginbotham, and C. Miller, "KcsA: It's a potassium channel," *J. Gen. Physiol.*, vol. 118, pp. 303–313, 2001.
- [30] R. J. Mashl, Y. Tang, J. Schnitzer, and E. Jakobsson, "Hierarchical approach to predicting permeation in ion channels," *Biophys. J.*, vol. 81, pp. 2473–2483, 2001.
- [31] D. Meuser, H. Splitt, R. Wagner, and H. Schrepf, "Exploring the open pore of the potassium channel from streptomyces lividans," *FEBS Lett.*, vol. 462, pp. 447–452, 1999.
- [32] C. Miller, "Open-state substructure of single chloride channels from torpedo electroplax," *Philos. Trans. R. Soc. London*, vol. B299, pp. 401–411, 1982.
- [33] G. V. Miloshevsky and P. C. Jordan, "Anion pathway and potential energy profiles along curvilinear bacterial CIC  $Cl^-$  pores: Electrostatic effects of charged residues," *Biophys. J.*, vol. 86, pp. 825–835, 2004.
- [34] G. Pflug, *Optimization of Stochastic Models: The Interface Between Simulation and Optimization*. Norwell, MA: Kluwer, 1996.
- [35] M. Pusch and T. Jentsch, "Unique structure and function of chloride transporting CIC proteins," *IEEE Trans. Nanobiosci.*, vol. 4, no. 1, pp. 49–57, Mar. 2005.
- [36] B. Roux and K. Schulten, "Computational studies of membrane channels," *Structure*, vol. 12, pp. 1343–1351, 2004.
- [37] A. Grottesi, C. Domene, S. Haider, and M. S. P. Sansom, "Molecular dynamics simulation approaches to K channels: Conformational flexibility and physiological function," *IEEE Trans. Nanobiosci.*, vol. 4, no. 1, pp. 112–120, Mar. 2005.
- [38] H. Schrepf, O. Schmidt, R. Kümerlen, S. Hinnah, D. Müller, M. Betzler, T. Steinkamp, and R. Wagner, "A prokaryotic potassium ion channel with two predicted transmembrane segment from streptomyces lividans," *EMBO J.*, vol. 14, pp. 5170–5178, 1995.
- [39] F. H. Stillinger and A. Rahman, "Improved simulation of liquid water by molecular dynamics," *J. Chem. Phys.*, vol. 60, pp. 1545–1557, 1974.
- [40] D. P. Tieleman, P. C. Biggin, G. R. Smith, and M. S. P. Sansom, "Simulation approaches to ion channel structure–function relationships," *Q. Rev. Biophys.*, vol. 34, pp. 473–561, 2001.
- [41] Y. Zhou, J. H. Morales-Cabral, A. Kaufman, and R. MacKinnon, "Chemistry of ion coordination and hydration revealed by a  $K^+$  channel-fab complex at 2.0 Å resolution," *Nature*, vol. 414, pp. 43–48, 2005.



**Vikram Krishnamurthy** (SM'99–F'05) was born in 1966. He received the B.S. degree in electrical engineering from the University of Auckland, New Zealand, in 1988 and the Ph.D. degree from the Australian National University, Canberra, in 1992.

He is currently a Professor and Canada Research Chair in the Department of Electrical Engineering, University of British Columbia, Vancouver, BC, Canada. Prior to 2002, he was a Chaired Professor in the Department of Electrical and Electronic Engineering, University of Melbourne, Australia,

where he also served as Deputy Head of Department. He is currently an Associate Editor for *Systems and Control Letters*. His current research interests include ion channels and biological nanotubes, networked sensor scheduling and control, statistical signal processing, nonlinear filtering, and wireless telecommunications.

Dr. Krishnamurthy is currently an Associate Editor for the IEEE TRANSACTIONS ON SIGNAL PROCESSING and the IEEE TRANSACTIONS ON AEROSPACE AND ELECTRONIC SYSTEMS. He is guest editor of a special issue of the IEEE TRANSACTIONS ON NANOBIOSCIENCE (March 2005) on bionanotubes. He currently serves on the Signal Processing Theory and Methods (SPTM) Technical Committee of the IEEE Signal Processing Society and the International Federation of Automatic Control (IFAC) Technical Committee on Modeling, Identification, and Signal Processing. He has served on the technical program committee of several conferences in signal processing, telecommunications, and control.



**Shin-Ho Chung** received the B.Sc. degree from Stanford University, Stanford, CA, in 1962 and the Ph.D. degree from Harvard University, Cambridge, MA, in 1966.

He held a postdoctoral position at the Massachusetts Institute of Technology, Cambridge. Currently, he is the Head of the Biophysics Group in the Department of Theoretical Physics, Australian National University, Canberra. His primary research effort is aimed at building theoretical models of biological ion channels.